Int. J. Heat Mass Transfer. Vol. 33, No. 10, pp. 2111–2120, 1990
Printed in Great Britain

0017–9310/90 $3.00 + 0.00

Multi-component interfacial condensation

F. M. GERNER† and C. L. TIEN‡
Department of Mechanical Engineering, University of California, Berkeley, CA 94720, U.S.A.

(*Received* 23 *February* 1989 *and in final form* 11 *December* 1989)

Abstract—This paper employs a simple laminar axisymmetric model to study multi-component condensation. In addition to including the complex phase equilibria inherent with multi-component condensation; interfacial shear stress, mass and energy transport are also considered. It is demonstrated that a non-condensable gas significantly reduces the interfacial condensation rate. For binary condensation, the freestream vapor concentration is very important. Higher concentrations of the more volatile component tend to inhibit condensation.

INTRODUCTION

THIS WORK analyzes the interfacial mass and energy transport occurring at the interface between the vapor and liquid phases of a multi-component mixture. It examines the condensation taking place on the surface of a subcooled liquid mixture, when there is sub-surface liquid motion. The geometry for this study is identical to the direct-contact forced-convective condensation above a circulating liquid pool used to analyze the pressurizer of a nuclear power plant [1]. Since the interactions between interfacial forces and interfacial mass fluxes are similar for all vapor–liquid interfaces, the model can be used to better understand the influence of convection near vapor–liquid interfaces in other geometries. For example, binary film condensation on flat plates and inside or outside tubes all exhibit very similar interfacial behavior.

While other investigators have examined interfacial pool condensation [1–6], none of their results have included multi-component condensation. Also there have been some studies of film condensation in the presence of a non-condensable gas [7–9], and binary film condensation [10–13]. None of these studies, however, have fully accounted for the complex dynamic coupling occurring at the vapor–liquid interface. In particular, they do not match the vapor and liquid shear stresses at the interface. For a relatively stagnant vapor, this is not necessary. For rapidly moving vapors, however, the subsequent high interfacial shear stress does affect the interfacial condensation rate. This work provides a simple, yet rigorous, model to demonstrate clearly how interfacial phenomena, such as interfacial shear stress and condensation mass flux, affect the velocity fields, interact with the complex phase equilibria, and hence affect the interfacial mass and energy transport.

The model to be analyzed is graphically represented in Fig. 1. A subcooled liquid flows axisymmetrically toward a flat gas–liquid interface. In general, the liquid is a binary mixture and the gas is a mixture of a superheated binary vapor and a non-condensable gas (the model will work equally well for more components). To satisfy the no-slip and force balance conditions at the interface the gas mixture must also be in motion. In order to simplify the formulation and to focus attention on the interface, steady-state axisymmetric laminar stagnation flows are assumed to exist in both the liquid and the mixture. Inviscid flow occurs in both fluids except for thin boundary layers on either side of the interface. By introducing

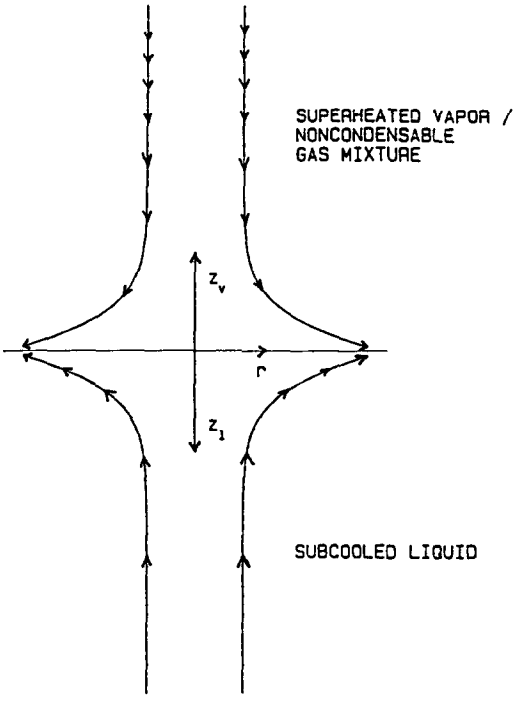

FIG. 1. Axisymmetric interfacial transport model.

† Present address: Department of Mechanical, Industrial and Nuclear Engineering, University of Cincinnati, Cincinnati, OH 45221, U.S.A.

‡ Present address: Department of Mechanical Engineering, University of California, Irvine, CA 92717, U.S.A.

NOMENCLATURE

a	stagnation parameter
C_i	constant, equation (6)
C_p	specific heat at constant pressure
D	binary diffusion coefficient
F	dimensionless similarity variable, equation (24)
g	gravitational acceleration
$h_{v\ell}$	latent heat of vaporization
$h(z)$	z-dependence of pressure, equation (26)
Ja	Jakob number, equation (22)
k	thermal conductivity
m	mass fraction
M	molecular weight
n	mole fraction
P	pressure
Pr	Prandtl number, equation (22)
r	radial coordinate
R	specific gas constant
Sc	Schmidt number, ν/D
T	temperature
u	radial or streamwise velocity
v	cross-stream velocity
w	axial velocity
x	streamwise coordinate
y	cross-stream coordinate
z	axial coordinate.

Greek symbols

α	thermal diffusivity
γ	activity coefficient, equation (15)
μ	dynamic viscosity
ν	kinematic viscosity
ρ	density.

Subscripts and superscripts

c	condensable substance
g	non-condensable gas
i	ℓ or v
j	substance index
ℓ	liquid
o	stagnation
p	number of substances
s	saturation
v	vapor
w	wall
∞	infinity
*	dimensionless, equation (20)
+	alternate nondimensionalization, equation (44)
′	differentiation w.r.t. z^*.

appropriate similarity variables, the governing equations can be transformed into a one-dimensional system of mathematical equations. Therefore, boundary conditions are required only in the direction normal to the interface. A numerical technique is employed to solve this system of equations.

Previously, the axisymmetric laminar-flow model has been used to study pure-component condensation. The effects of interfacial forces, subcooling of the liquid, and superheating of the vapor have all been examined for pure-component condensation [1]. Some of these results will be used to simplify the analysis of multi-component condensation.

The next section outlines the mathematical formulation. After introducing the numerical procedure used, multi-component condensation is examined. For multi-component condensation, the physics and mathematics become slightly more complicated than for pure-component condensation. For multi-component condensation the phase equilibria at the interface is very important. Two cases are studied: condensation when there is a non-condensable gas present in the vapor, and condensation of a binary mixture. A non-condensable gas tends to accumulate at the interface as the vapor condenses. This offers a diffusion barrier to the vapor which inhibits condensation. Another way to think of this is that large concentrations of a non-condensable gas lower the partial vapor pressure and saturation temperature. Hence the subcooling is effectively lowered. It is then shown that binary condensation is primarily controlled by thermal transport in the liquid and mass transport in the vapor. It is interesting, that by altering the vapor concentrations, the same condensation rate can be achieved using different liquid temperatures.

Before introducing the model it is important to re-emphasize that while this work closely models the direct contact condensation above a circulating liquid pool, it has much wider relevance. The same interaction between interfacial forces and interfacial mass fluxes occur near all vapor–liquid condensation interfaces. The reason is that interfacial heat and mass transfer is a very local phenomenon. Of course for other applications, such as binary laminar-film condensation, the non-interface boundary conditions are different. But the relationship between the dynamics and mass and energy transfer near the interface is very similar.

FORMULATION

The following equations governing conservation of mass, momentum, energy and species are for constant density and constant transport properties of the pure substances:

$$\frac{\partial u_i}{\partial r} + \frac{u_i}{r} + \frac{\partial w_i}{\partial z_i} = 0 \tag{1}$$

$$u_i\frac{\partial u_i}{\partial r}+w_i\frac{\partial u_i}{\partial z_i}=\frac{-1}{\rho_i}\frac{\partial P_i}{\partial r}+\nu_i\left(\frac{\partial^2 u_i}{\partial r^2}+\frac{1}{r}\frac{\partial u_i}{\partial r}-\frac{u_i}{r^2}+\frac{\partial^2 u_i}{\partial z_i^2}\right) \quad (2)$$

$$u_i\frac{\partial w_i}{\partial r}+w_i\frac{\partial w_i}{\partial z_i}=\frac{-1}{\rho_i}\frac{\partial P_i}{\partial z_i}+\nu_i\left(\frac{\partial^2 w_i}{\partial r^2}+\frac{1}{r}\frac{\partial w_i}{\partial r}+\frac{\partial^2 w_i}{\partial z_i^2}\right)\pm g \quad (3)$$

$$w_i\frac{\mathrm{d}T_i}{\mathrm{d}z_i}=\alpha_i\frac{\mathrm{d}^2T_i}{\mathrm{d}z_i^2} \quad (4)$$

$$w_i\frac{\mathrm{d}m_{i(j)}}{\mathrm{d}z_i}=D_i\frac{\mathrm{d}^2m_{i(j)}}{\mathrm{d}z_i^2} \quad (5)$$

where, in the z-direction momentum equation, the '+' is for the liquid and the '−' for the vapor (numerically it is more convenient to use different coordinate systems on either side of the interface). Diffusion-thermo and thermo-diffusive effects have been neglected and it is assumed that multi-component mixtures can be characterized by a single diffusion coefficient (the model can handle non-equal diffusion coefficients, but Fick's law is not valid and the equations change). From the Clausius–Clapeyron relation [14], and the known pressure gradients, it can be shown that the saturation temperature is constant along the interface. Hence temperature and mass fraction are only functions of distance from the interface.

The far fields ($z_i \to \infty$) are assumed to be inviscid uniform flows

$$u_i = a_i r, \quad w_i = -2a_i z_i + C_i \quad (6)$$

$$T_i = T_{i\infty}, \quad m_{i(j)} = m_{i(j)\infty}. \quad (7)$$

At the interface ($z_v = z_\ell = 0$), the conditions are

$$u_\ell = u_v, \quad -\rho_\ell w_\ell = \rho_v w_v \quad (8)$$

$$P_\ell - 2\mu_\ell\frac{\partial w_\ell}{\partial z_\ell} = P_v - 2\mu_v\frac{\partial w_v}{\partial z_v},$$

$$-\mu_\ell\left(\frac{\partial w_\ell}{\partial r}+\frac{\partial u_\ell}{\partial z_\ell}\right)=\mu_v\left(\frac{\partial w_v}{\partial r}+\frac{\partial u_v}{\partial z_v}\right) \quad (9)$$

$$T_\ell = T_v = T_s,$$

$$-k_\ell\frac{\mathrm{d}T_\ell}{\mathrm{d}z_\ell}=\sum_{j=1}^{p}\left(\rho_{\ell(j)}w_\ell-\rho_\ell D_\ell\frac{\partial m_{\ell(j)}}{\partial z_\ell}\right)h_{v\ell(j)}+k_v\frac{\mathrm{d}T_v}{\mathrm{d}z_v} \quad (10)$$

$$-\rho_v D_v\frac{\partial m_{v(j)}}{\partial z_v}+\rho_{v(j)}w_v=\rho_\ell D_\ell\frac{\partial m_{\ell(j)}}{\partial z_\ell}-\rho_{\ell(j)}w_\ell. \quad (11)$$

Equations (8) represent the no-slip and conservation of mass conditions, equations (9) force balances, equations (10) continuity of temperature (neglecting the interfacial resistance) and conservation of energy, and equation (11) conservation of species. Additionally the thermodynamic relation between the saturation temperature and interfacial mass fractions is required to couple the interface conditions.

For this analysis, the pure-component saturation curves are assumed to obey the simple Clapeyron equation [14]

$$\left(\frac{\mathrm{d}P_s}{\mathrm{d}T_s}\right)_{(j)}=\left[\frac{h_{v\ell}}{T_s(1/\rho_v-1/\rho_\ell)}\right]_{(j)}. \quad (12)$$

Neglecting the specific volume of the liquid ($1/\rho_\ell$) relative to that of the vapor ($1/\rho_v$), which is a good assumption except near the critical point, assuming h_{vl} is constant, and using the ideal gas law

$$\frac{P}{\rho}=RT \quad (13)$$

yields

$$\frac{P_{s(j)}}{P_v}=\exp\left[-\frac{h_{v\ell(j)}}{R_{v(j)}}(1/T_s-1/T_{s(j)}(P_v)\right]. \quad (14)$$

Representing the phase equilibria as

$$n_{v(j)}P_v=\gamma_j(T,P)n_{\ell(j)}P_{s(j)} \quad (15)$$

where $\gamma_j(T,P)$ is the activity coefficient [11]. Therefore

$$\frac{n_{v(j)}}{n_{\ell(j)}}=\gamma_j(T,P)\exp\left[-\left(\frac{h_{v\ell}}{R_vT_s(P_v)}\right)_{(j)}\times\left(\frac{T_{s(j)}(P_v)}{T_{s(1)}(P_v)}\frac{T_{s(1)}(P_v)}{T_s}-1\right)\right]. \quad (16)$$

Note that using the activity coefficient in this form is mostly for mathematical closure. For condensation in the presence of a non-condensable gas, a simpler phase equilibrium relation is used. For binary condensation a graphical representation is used. Conservation of moles, mass and Dalton's law are necessary for closure

$$\sum_{j=1}^{p}n_{i(j)}=1 \quad (17)$$

$$m_{i(j)}=\frac{n_{i(j)}\dfrac{M_j}{M_1}}{\displaystyle\sum_{j=1}^{p}n_{i(j)}\frac{M_j}{M_1}} \quad (18)$$

$$\sum_{j=1}^{p}P_{v(j)}=P_v. \quad (19)$$

Introducing the dimensionless quantities ($m_{i(j)}$ are already dimensionless)

$$u_i^* = u_i(\nu_i a_i)^{-1/2}, \quad w_i^* = w_i(\nu_i a_i)^{-1/2}$$

$$r_i^* = r(\nu_i/a_i)^{-1/2}, \quad z_i^* = z_i(\nu_i/a_i)^{-1/2}$$

$$T_i^* = \frac{T_i - T_{i\infty}}{T_{s(1)}(P_v)-T_{i\infty}} \quad (20)$$

the following dimensionless parameters result.

Fluid mechanical

$$\frac{\mu_{v(1)}}{\mu_{\ell(1)}}, \quad \frac{\rho_{v(1)}(P_v)}{\rho_{\ell(1)}}. \quad (21)$$

Thermal

$$Ja_{i(1)} = \pm \frac{C_{pi(1)}(T_{s(1)}(P_v) - T_{i\infty})}{h_{v\ell(1)}}, \quad Pr_i = \frac{\nu_{i(1)}}{\alpha_{i(1)}} \tag{22}$$

where the '+' is for liquid and the '−' for vapor.

Species

$$Sc_i,\ m_{i(j)\infty},\ \frac{M_{(j)}}{M_{(1)}},\ \frac{\mu_{i(j)}}{\mu_{i(1)}},\ \frac{C_{pi(j)}}{C_{pi(1)}},\ \frac{h_{v\ell(j)}}{h_{v\ell(1)}}$$

$$\frac{k_{i(j)}}{k_1},\ \left[\frac{h_{v\ell}}{R_v T_s(P_v)}\right]_{(j)},\ \frac{T_{i\infty}}{T_{s(1)}(P_v)},\ \frac{T_{s(j)}(P_v)}{T_{s(1)}(P_v)}. \tag{23}$$

The following similarity solutions, which satisfy continuity identically, exist

$$u_i^* = r_i^* \frac{dF_i(z_i^*)}{dz_i^*}, \quad w_i^* = -2F_i(z_i^*). \tag{24}$$

Substitution into the z-direction momentum equations, and differentiation with respect to r, yields

$$\frac{\partial^2 P_i}{\partial r\, \partial z_i} = 0 \tag{25}$$

which implies that, if P_i is continuously differentiable, $\partial P_i/\partial r$ is not a function of z_i and can be evaluated from the inviscid far field

$$P_\infty - P_i = 1/2\rho_i(a_i^2 r^2 + h_i(z)) \tag{26}$$

and by equating radial pressure gradients at the interface (radial pressure gradients can be seen to be equal by differentiating equation (9) with respect to r)

$$a_\ell/a_v = (\rho_v/\rho_\ell)^{1/2} \tag{27}$$

where ρ_v/ρ_ℓ is assumed constant and equal to the interface value. It is evaluated using the ideal gas law as

$$\frac{\rho_v}{\rho_\ell} = \frac{\rho_{v(1)}(P_v)}{\rho_{\ell(1)}(P_v)} \frac{n_{v(1)}}{m_{v(1)}} \sum_{j=1}^{p} m_{\ell(j)} \frac{\rho_{\ell(1)}(P_v)}{\rho_{\ell(j)}(P_v)}. \tag{28}$$

The transformed momentum and energy equations in similarity form become

$$\left(\frac{dF_i}{dz_i^*}\right)^2 - 2F_i \frac{d^2F_i}{dz_i^{*2}} = 1 + \frac{d^3F_i}{dz_i^{*3}} \tag{29}$$

$$-2Pr_i F_i \frac{dT_i^*}{dz_i^*} = \frac{d^2T_i^*}{dz_i^{*2}} \tag{30}$$

where the mixture Prandtl number is defined as

$$\frac{Pr_i}{Pr_{i(1)}} = \frac{\left(\sum_{j=1}^{p} n_{i(j)} \frac{u_{i(j)}}{\mu_{i(1)}}\right)\left(\sum_{j=1}^{p} m_{i(j)} \frac{C_{pi(j)}}{C_{pi(1)}}\right)}{\sum_{j=1}^{p} n_{i(j)} \frac{k_{i(j)}}{k_{i(1)}}}. \tag{31}$$

These are complemented by the species equation

$$-2Sc_i F_i \frac{dm_{i(j)}}{dz_i^*} = \frac{d^2 m_{i(j)}}{dz_i^{*2}} \tag{32}$$

Sc_i being treated as a constant.

Boundary conditions for the above equations are, as z approaches infinity

$$dF_i/dz_i^* = 1, \quad T_i^* = 0, \quad m_{i(j)} = m_{i(j)\infty} \tag{33}$$

while matching conditions at the interface are

$$\frac{dF_\ell}{dz_\ell^*} = \left(\frac{\rho_\ell}{\rho_v}\right)^{1/2} \frac{dF_v}{dz_v^*} \tag{34}$$

$$F_\ell = -\left(\frac{\rho_v}{\rho_\ell}\right)^{1/4} \left(\frac{\mu_v}{\mu_\ell}\right)^{1/2} F_v \tag{35}$$

$$-\frac{d^2F_\ell}{dz_\ell^{*2}} = \left(\frac{\mu_v}{\mu_\ell}\right)^{1/2} \left(\frac{\rho_\ell}{\rho_v}\right)^{1/4} \frac{d^2F_v}{dz_v^{*2}} \tag{36}$$

$$\frac{C_{p\ell}}{C_{pv(1)}} \frac{Ja_{\ell(1)}}{Pr_\ell} \frac{dT_\ell^*}{dz_\ell^*} = \sum_{j=1}^{p} \left(2m_{\ell(j)} F_\ell + \frac{1}{Sc_\ell} \frac{dm_{\ell(j)}}{dz_\ell^*}\right) \frac{h_{v\ell(j)}}{h_{v\ell(1)}} + \left(\frac{\rho_v}{\rho_\ell}\right)^{1/4} \left(\frac{\mu_v}{\mu_\ell}\right)^{1/2} \frac{C_{pv}}{C_{pv(1)}} \frac{Ja_{v(1)}}{Pr_v} \frac{dT_v^*}{dz_v^*} \tag{37}$$

$$2F_\ell(m_{\ell(j)} - m_{v(j)}) + \frac{1}{Sc_\ell} \frac{dm_{\ell(j)}}{dz_\ell^*} + \left(\frac{\mu_v}{\mu_\ell}\right)^{1/2} \left(\frac{\rho_v}{\rho_\ell}\right)^{1/4} \frac{1}{Sc_v} \frac{dm_{v(j)}}{dz_v^*} = 0 \tag{38}$$

$$T_i^* = \frac{T_s - T_{i\infty}}{T_{s(1)}(P_v) - T_{i\infty}} \tag{39}$$

where the mixture specific heat at constant pressure and dynamic viscosity are defined as

$$\frac{C_{pi}}{C_{pi(1)}} = \sum_{j=1}^{p} m_{i(j)} \frac{C_{pi(j)}}{C_{pi(1)}} \tag{40}$$

$$\frac{\mu_v}{\mu_\ell} = \frac{\mu_{v(1)}}{\mu_{\ell(1)}} \frac{\sum_{j=1}^{p} n_{v(j)} \frac{\mu_{v(j)}}{\mu_{v(1)}}}{\sum_{j=1}^{p} n_{\ell(j)} \frac{\mu_{\ell(j)}}{\mu_{\ell(1)}}}. \tag{41}$$

NUMERICAL SOLUTION

Of primary importance in this study is the interfacial condensation rate. An order of magnitude estimate of this parameter can be obtained from the inviscid pure-component condensation solution [1]

$$-F_\ell(0) = Ja_\ell(\pi\, Pr_\ell)^{-1/2}. \tag{42}$$

Precise numerical results for multi-component condensation, however, require solution of equations (29), (30) and (32) along with far field conditions (33) and interface conditions (34)–(39). Additionally the thermodynamic relation, equation (16). its auxiliary equations (17)–(19) and multi-component mixture property relations, equations (28), (31). (40) and (41), are required. It is now apparent why z_v and z_ℓ were used. Since one boundary condition is at infinity for both the gas mixture and the liquid, and the gas field equations are decoupled from the liquid field equations (except at the interface), what is physically a three-point boundary-value problem can be represented mathematically as a two-point boundary-value problem (the two boundaries, $z_v^* \to \infty$, $z_\ell^* \to \infty$,

merge to simply $z^* \to \infty$, and the interface conditions can be treated mathematically as coupled boundary conditions at $z^* = 0$).

The resulting system of non-linear ordinary differential equations has no known closed form solution; therefore it must be solved numerically. It should be noted that the general problem of binary condensation with a non-condensable gas is a system of seven ordinary differential equations, two of which are third order and five are second order. There are seven infinity conditions, nine interface conditions and eight auxiliary relations. To attempt to blindly solve this system would be extremely difficult. Clearly a more intelligent approach is necessary. Due to the nondimensionalization, the freestream velocity is not a parameter in this problem. Basically, after choosing the substances and total pressure there are only five free parameters. They are the liquid freestream temperature (or $Ja_{\ell(1)}$), gas freestream temperature ($Ja_{v(1)}$), liquid freestream concentration for the second component ($m_{\ell(2)}$), vapor freestream concentration for the second component ($m_{v(2)}$) and freestream non-condensable gas fraction ($m_{v(g)\infty}$). They act as the driving potentials and determine the conditions at the interface $F_\ell(0)$, $m_{i(j)}(0)$ and T_s. However, to solve the problem in this fashion is very difficult. Instead interface conditions $F_\ell(0)$, T_s and $dm_{\ell(j)}/dz_\ell^*$ (for the non-condensable gas this is zero) are chosen and the driving potentials which yield these conditions are determined. Koh [15] used a similar procedure to determine the Jakob number for forced-convective condensation onto a flat plate.

The first step is to choose the condensable and non-condensable substances, the total pressure (P_v) and corresponding saturation temperature ($T_{s(1)}(P_v)$). All dimensionless parameters given by equations (21)–(23), except for $Ja_{i(1)}$, $m_{i(j)\infty}$ and $T_{i\infty}/T_{s(1)}(P_v)$ are determined. Choosing T_s fixes $m_{i(j)}(0)$ and, assuming all pure-component properties are constant and equal to their interface values, allows the mixture properties to be determined using equations (28), (31), (40) and (41). Specifying $F_\ell(0)$ allows the momentum equations to be solved independent of the energy and species equations.

The momentum equations are solved first. Once $F_\ell(0)$ is specified, they are given by equations (29), (33), (34), (36) and

$$F_v(0) = -\left(\frac{\rho_\ell}{\rho_v}\right)^{1/4}\left(\frac{\mu_\ell}{\mu_v}\right)^{1/2} F_\ell(0). \tag{43}$$

In order to solve this system a shooting technique was used [16]. The equations were first expressed as a system of first-order ODEs. $F_\ell'(0)$ and $F_\ell''(0)$ were guessed, equations (34) and (36) used to calculate $F_v'(0)$ and $F_v''(0)$ and a fourth-order adaptive-step-size Runge–Kutta scheme was used to shoot to the infinity boundary; normally $z^* = 10$ is sufficient. Finally a Newton–Raphson technique was used to match the infinity conditions, given by equations (33).

Once the $F_i(z^*)$ are known the energy equations are solved. New dimensionless temperatures are introduced

$$T_i^+ = \frac{T_i - T_{i\infty}}{T_s - T_{i\infty}} = T_i^* \frac{T_s(P_v) - T_{i\infty}}{T_s - T_{i\infty}} \tag{44}$$

and the energy equation then becomes

$$-2Pr_i F_i T_i^{+\prime} = T_i^{+\prime\prime} \tag{45}$$

with boundary conditions

$$T_i^+(0) = 1, \quad T_i^+(\infty) = 0. \tag{46}$$

By using a shooting technique similar to that used for the momentum equations, $T_i^{+\prime}(0)$ can be found. Knowing $T_i^{+\prime}(0)$, thermophysical properties and using equation (37) allows calculation of $Ja_{\ell(1)}$ and $Ja_{v(1)}$. Actually there are many combinations of $Ja_{\ell(1)}$ and $Ja_{v(1)}$ which are possible for a given condensation rate. In other words, the condensation rate is not solely a function of the liquid subcooling. Large vapor superheats can significantly reduce the interfacial condensation rate. Finally $m_{i(j)}(0)$, $dm_{\ell(j)}(0)/dz_\ell^*$ and equations (32) and (38) are used to calculate the $m_{i(j)\infty}$ using a simple shooting routine.

RESULTS

In order to obtain some understanding of how mixture concentration alters the interfacial phase equilibria, and hence the interfacial condensation rate, condensation in the presence of a non-condensable gas will be examined. The particular system studied will be the condensation of water vapor which contains some air. By restricting attention to the air/water system, many of the dimensionless parameters given in equations (21)–(23) are fixed. Therefore, their effect upon the condensation process cannot be seen. For the majority of these parameters, however, the primary effect is to alter the thermophysical and transport properties of the mixture. How this affects the interfacial condensation rate was discussed in ref. [1].

For the condensation of an atmospheric mixture of water vapor and air, in addition to the liquid subcooling, the freestream or non-condensable gas fraction, $m_{v,g\infty}$, is also very important. The way that the non-condensable gas concentration affects the interfacial condensation rate is more interesting than simply affecting the thermophysical properties. By lowering the partial pressure of the vapor at the interface, it decreases the effective subcooling and hence inhibits condensation. The dimensionless parameters for an atmospheric water/air system are shown in Table 1 [17]. The thermodynamic relation, equation (16), is simplified in that the liquid mole fraction for water and the activity coefficient are both identically 1. This is consistent with assuming that air is a non-condensable gas. Also, since the effects of vapor superheat have been shown to be small [1], it has been neglected.

Figure 2 shows both the interfacial non-condensable gas fraction, $m_{v,air}(0)$, and interfacial satu-

Table 1. Saturated steam air mixture properties at atmospheric pressure

Fluid mechanical	
$\frac{\mu_{v,H_2O}}{\mu_\ell}$	4.26×10^{-2}
$\frac{\rho_{v,H_2O}(P_v)}{\rho_\ell}$	6.24×10^{-4}
Subcooling	
Pr_ℓ	1.75
Superheat	
Pr_{v,H_2O}	0.987
Non-condensable gas	
Sc_v	0.6
$\frac{M_{v,air}}{M_{v,H_2O}}$	1.608
$\frac{\mu_{v,air}}{\mu_{v,H_2O}}$	1.802
$\frac{C_{pv,air}}{C_{pv,H_2O}}$	0.497
$\frac{k_{v,air}}{k_{v,H_2O}}$	1.273
$\left[\frac{h_{v\ell}}{R_v T_{sat}(P_v)}\right]_{H_2O}$	13.105

ration temperature as functions of non-condensable gas fraction at infinity, $m_{v,air\infty}$, for $F_\ell(0) = -10^{-2}$. As can be seen $m_{v,air}(0)$ is almost directly related to $m_{v,air\infty}$. In other words, a small freestream non-condensable gas fraction produces a much larger interfacial non-condensable gas fraction. The exponential relationship, equation (16), between $m_{v,air}(0)$ and $T_s/T_s(P_v)$ somewhat dampens the effect upon the interfacial saturation temperature.

Figure 3, however, shows that the subcooling necessary to maintain this condensation rate increases greatly as the freestream non-condensable gas fraction is increased. Also since the slope of the curve is rapidly increasing it is seen that for large non-condensable gas fractions, slight changes have a dramatic effect upon the subcooling required to maintain condensation.

In some respects, binary condensation is very similar to condensation in the presence of a non-condensable gas. In addition to mass diffusion in the vapor phase, however, there is mass diffusion in the liquid, and additionally the phase equilibrium at the interface is more complicated. In a sense, binary condensation is the general case and condensation in the presence of a non-condensable gas may be thought of as a special case.

To make things a little more concrete, an atmospheric methanol–water mixture was chosen to be the binary mixture. Their mixture properties are shown in Table 2 [17, 18]. In lieu of equation (16) the equilibrium curve shown in Fig. 4, taken from Sparrow and Marschall [12], is used to determine the phase equilibrium at the interface.

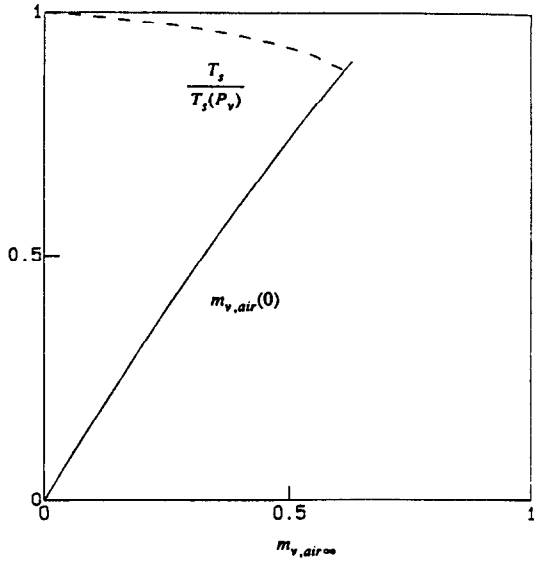

FIG. 2. The effects of mass diffusion upon interface conditions for atmospheric air/stream mixture.

Conceptually it is easier to think of the less volatile component, water, as condensing more rapidly. In order to be in steady state in the axisymmetric configuration the mole fraction of methanol must be largest at the interface. Otherwise convection and diffusion would both bring methanol vapor toward the interface. Since it is not condensing as fast as the water it would build up at the interface. This is similar to the case where convection brought both the vapor and non-condensable gas to the interface, the vapor condensed and the non-condensable gas diffused back

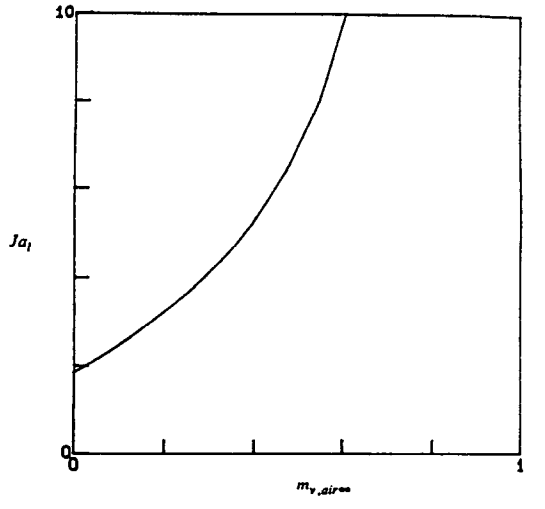

FIG. 3. Relationship between subcooling and non-condensable air fraction for atmospheric water.

Table 2. Binary water/methanol mixture properties at atmospheric pressure

Fluid mechanical			
$\frac{\mu_{v,H_2O}}{\mu_{\ell,H_2O}}$	4.26×10^{-2}		
$\frac{\rho_{v,H_2O}(P_v)}{\rho_{\ell,H_2O}}$	6.24×10^{-4}		
Subcooling			
Pr_{ℓ,H_2O}	1.75		
Superheat			
Pr_{v,H_2O}	0.987		
Binary			
Sc_v	0.6	Sc_ℓ	8250
$\frac{\mu_{v,meth}}{\mu_{v,H_2O}}$	0.9646	$\frac{\mu_{\ell,meth}}{\mu_{\ell,H_2O}}$	0.8393
$\frac{C_{pv,meth}}{C_{pv,H_2O}}$	0.9229	$\frac{C_{p\ell,meth}}{C_{p\ell,H_2O}}$	0.7463
$\frac{k_{v,meth}}{k_{v,H_2O}}$	0.9085	$\frac{k_{\ell,meth}}{k_{\ell,H_2O}}$	0.2912
$\frac{M_{meth}}{M_{H_2O}}$	1.7779		
$\frac{h_{v\ell,meth}}{h_{v\ell,H_2O}}$	0.4462		

away from the interface. For the liquid side, the Lewis number is very large ($Le_\ell = \alpha_\ell/D_\ell = 4000$). Therefore, the diffusive boundary layer is much smaller than the thermal boundary layer. The diffusive region is at approximately constant temperature equal to the interface or saturation temperature. Since condensation is occurring at the interface, the concentration of methanol must be largest there.

A typical example of a concentration profile is

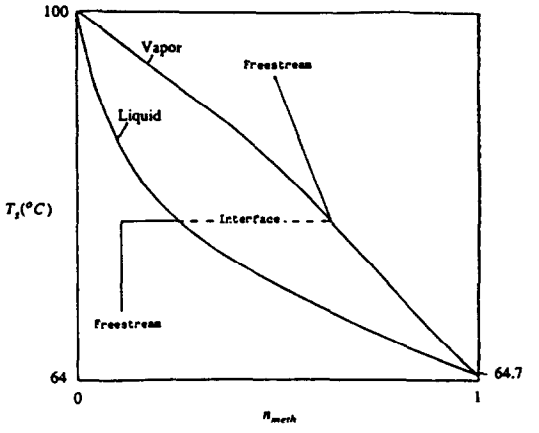

FIG. 4. Typical relationship between interface and freestream concentrations near a methanol/water condensing interface.

shown in Figs. 4 and 5. What these figures demonstrate, is that the concentration varies throughout the momentum boundary layer in the vapor. In the liquid, however, the concentration is almost uniform except for a very tiny region next to the interface. In other words, for such a large liquid Schmidt number, the concentration boundary layer is much smaller than the momentum boundary layer.

Some typical results were run for $\dot{F}_\ell(0) = -10^{-2}$ and are shown in Table 3. The first thing to notice is that the condensation rate and actual subcooling are intimately related. Practically the same temperature difference between the liquid freestream and interface produces a given condensation rate independent of absolute temperature. The other thing to notice is that a given saturation temperature and condensation rate can be achieved with many different liquid freestream concentrations, while the vapor freestream concentration cannot vary much and the liquid freestream temperature is essentially constant.

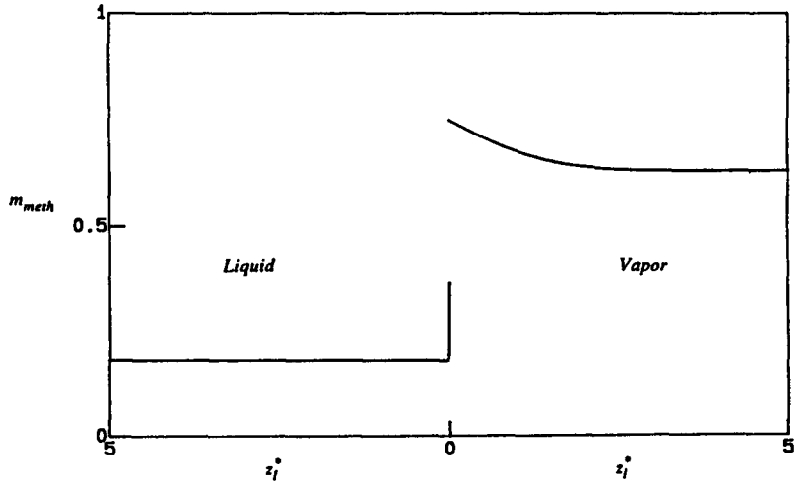

FIG. 5. Concentration profile with $m_{\ell\infty} = 0.1845$, $m_{v\infty} = 0.6312$, and $T_{\ell\infty} = 71.23$°C.

Table 3. Freestream conditions which yield the same condensation rate for a water/methanol binary mixture

T_s(°C)	$m_{\ell,\infty}$	$-F_\ell(0) = 10^{-2}$ $m_{v,\infty}$	$T_{\ell,\infty}$(°C)
64.7	1.0000	1.0000	55.87
72	0.1240	0.8832	64.95
	0.2312	0.8710	64.69
	0.3243	0.8604	64.46
	0.4174	0.8499	64.22
	0.5106	0.8393	63.99
	0.6037	0.8287	63.76
	0.6968	0.8181	63.53
80	0.0016	0.6535	71.61
	0.1845	0.6312	71.23
	0.3674	0.6089	70.84
88	0.0042	0.4301	78.69
	0.0400	0.4254	78.62
	0.0757	0.4208	78.55
	0.1651	0.4092	78.37
96	0.0005	0.1685	86.27
	0.0178	0.1659	86.24
	0.0525	0.1610	86.17
100	0.0000	0.0000	90.10

Of course, this should not be too surprising since the third term in equation (38) is a couple of orders of magnitude larger than the second term. As long as there is appreciable condensation then, right at the interface, almost all of the mass transport in the liquid is due to convection. Since the liquid mass diffusion region is small compared with both the momentum and thermal boundary layers (the Schmidt and Lewis numbers are large), mass diffusion has little influence on the velocity and thermal fields. As long as it is physically possible, the liquid concentration profile can adjust itself without greatly affecting anything else.

In a more general sense, this supports the observation [19] that the unmixed model works well for binary film condensation. In the unmixed model there is assumed to be no diffusion in the liquid right at the interface, consequently the concentration gradient, in the liquid, at the interface is zero. The concentration changes very rapidly in a tiny region near the interface to match the bulk concentration in the liquid phase. The boundary-layer region of the axisymmetric model can be thought of as this near-interface region. The reason why they are so similar is that, due to the high liquid Schmidt number, the concentration boundary layer is confined to a region so near to the interface that it is independent of the liquid velocity field (see Figs. 4 and 5).

Of course since this is a laminar-flow model, the mixed-flow model is not expected to work. For turbulent-film condensation it is often assumed that the liquid is so well mixed that the concentration is uniform throughout the liquid. For the axisymmetric model, unlike film condensation, the freestream liquid concentration is an independent variable. If the liquid concentration did not vary, however, this would fix the interface temperature, the liquid subcooling and hence the interfacial condensation rate. As has been shown, however, the interfacial condensation rate is not highly dependent on the liquid freestream concentration.

In demonstrating that for the axisymmetric model, and other laminar flow cases, that liquid freestream concentration is unimportant, and that liquid interfacial diffusion can be neglected, it has been assumed that the condensation is thermally induced. Therefore, the concentration gradient in equation (37) can be neglected relative to the thermal gradient in the liquid. If the subcooling in the liquid is small, however, this is no longer true. In fact, if Ja_ℓ/Pr is small enough, relative to $1/Sc_\ell$, phase change is driven by concentration gradients and not by thermal gradients. In this case, the concentration gradients in the liquid are no longer negligible and freestream liquid concentration is important. This effect has been noted by other investigators [19, 20], and is why Peterson *et al.* [19] found that neither the mixed or unmixed model worked very well for modeling the adiabatic section of their binary thermosyphon.

In order to simplify things somewhat the case where the concentration does not vary in the liquid ($dm_{\ell,\text{meth}}/dz^* = 0$) is examined. This would be one possible solution for methanol–water (the others would be similar except for the concentration profile in the liquid) and the only solution for an infinite Schmidt number.

These results are shown in Fig. 6. Note that the same condensation rate can be achieved with many different combinations of liquid freestream temperature (or saturation temperature) and freestream vapor concentration. Also the effects of changing either parameter can be seen from this figure. Basically anything which increases the actual subcooling increases the condensation rate. Lowering the liquid freestream temperature will, therefore, increase the

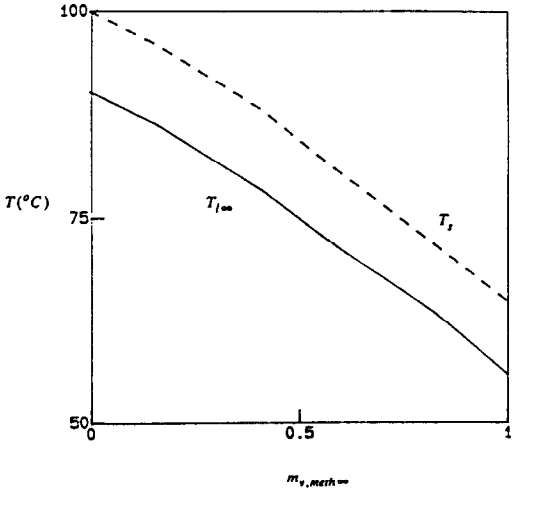

FIG. 6. Relationship between freestream vapor concentration and saturation and liquid freestream temperatures.

condensation rate. Decreasing the freestream mass fraction of methanol will tend to raise the saturation temperature, increase the subcooling, and increase the condensation rate.

CONCLUSIONS

In this work a simple axisymmetric model is used to study multi-component interfacial condensation. A one-dimensional system of equations is solved numerically. Of special interest is how interfacial mass and momentum balances affect the velocity and temperature fields which interact with the interfacial phase equilibrium to affect the interfacial condensation rate.

Previously, interfacial mass and energy transport have been studied for pure-component condensation. It had been determined how the vapor alters the velocity field in the liquid, changes the effective liquid subcooling, and hence alters the interfacial condensation rate. The purpose of this work was to examine how the presence of more than one fluid component alters the condensation rate. It accomplishes this by creating concentration gradients in the fluids and by altering the interfacial thermodynamics and phase equilibrium.

The presence of a non-condensable gas in the vapor significantly alters the relationship between the liquid subcooling and the condensation rate. By lowering the interfacial saturation temperature, a non-condensable gas significantly reduces condensation. For binary condensation, the freestream vapor concentration is very important. The higher the concentration of the more volatile component, the lower is the saturation temperature and effective subcooling. Hence higher concentrations of the more volatile component tend to inhibit condensation. Also it is shown why, for laminar liquid flow, the unmixed-flow model can be used to greatly simplify the interfacial phase equilibria.

REFERENCES

1. F. M. Gerner and C. L. Tien, Axisymmetric interfacial condensation model, presented at the Twenty-fifth National Heat Transfer Conf., 24–27 July, Houston, Texas (1988).
2. S. Banerjee, A surface renewal model for interfacial heat and mass transfer in transient two-phase flow, *Int. J. Multiphase Flow* **4**, 571–573 (1978).
3. G. P. Celata, M. Cumo, G. E. Farello and G. Focardi, Direct contact condensation of superheated steam on water, *Int. J. Heat Mass Transfer* **30**, 449–458 (1987).
4. G. P. Celata, M. Cumo, G. E. Farello and G. Focardi, A theoretical model of direct contact condensation on a horizontal surface, *Int. J. Heat Mass Transfer* **30**, 459–467 (1987).
5. O. C. Jones, Condensation heat transfer at an agitated steam–water interface, ASME Paper No. 66-Wa/HT-42 (1966).
6. R. M. Thomas, Condensation of steam on water in turbulent motion, *Int. J. Multiphase Flow* **5**, 1–15 (1979).
7. E. M. Sparrow, W. J. Minkowycz and M. Saddy, Forced convection condensation in the presence of noncondensables and interfacial resistance, *Int. J. Heat Mass Transfer* **10**, 1829–1845 (1967).
8. W. J. Minkowycz and E. M. Sparrow, Condensation heat transfer in the presence of non-condensibles, interfacial resistance, superheating, variable properties, and diffusion, *Int. J. Heat Mass Transfer* **9**, 1125–1144 (1966).
9. E. M. Sparrow and S. H. Lin, Condensation heat transfer in the presence of a noncondensable gas, *J. Heat Transfer* **86**(3), 430–436 (1964).
10. Y. Taitel and A. Tamir, Film condensation of multicomponent mixtures, *Int. J. Multiphase Flow* **1**, 697–714 (1974).
11. S. Kotake, Effects of a small amount of noncondensable gas on film condensation of multicomponent mixtures, *Int. J. Heat Mass Transfer* **28**, 407–414 (1985).
12. E. M. Sparrow and E. Marschall, Binary gravity-flow film condensation, *J. Heat Transfer* **91**, 205–211 (1969).
13. E. Tsotsas and E. U. Schluender, Heat transfer during evaporation and condensation of binary mixtures, *Chem. Engng Process.* **21**, 209–215 (1987).
14. H. B. Callen, *Thermodynamics and an Introduction to Thermostatistics*, pp. 228–231. Wiley, New York (1985).
15. J. C. Y. Koh, Film condensation in a forced-convective boundary-layer flow, *Int. J. Heat Mass Transfer* **5**, 941–954 (1962).
16. W. H. Press, B. P. Flannery, S. A. Teukolsky and W. T. Vetterling, *Numerical Recipes*, Chaps 15 and 16. Cambridge University Press, Cambridge (1986).
17. R. H. Perry, D. Green and J. O. Maloney, *Perry's Chemical Engineers' Handbook* (6th Edn), pp. 3-256–3-259. McGraw-Hill, New York (1984).
18. *ASHRAE Handbook, Fundamentals*, Chap. 17. ASHRAE, Atlanta, Georgia (1981).
19. P. F. Peterson, K. Hijikata and C. L. Tien, Variable-conductance behavior in two-phase binary thermosyphons, presented at the Ninth Int. Heat Transfer Conf., Jerusalem, Israel (August 1990).
20. K. Hijikata, Y. Mori, N. Himeno, M. Ingawa and K. Takahasi, Free convective condensation of a binary mixture of vapors, *Proc. 8th Int. Heat Transfer Conf.*, Vol. 4, pp. 1621–1626. Hemisphere, New York (1986).

CONDENSATION INTERFACIALE DANS LES MELANGES DE COMPOSANTS

Résumé—On emploie un modèle simple axisymétrique laminaire pour étudier la condensation de mélanges. Pour inclure l'équilibre complexe des phases dans cette condensation à plusieurs composants, on considère les taux de contraintes interfaciales, le transfert de chaleur et de masse. On montre qu'un gaz incondensable réduit sensiblement le flux interfacial de condensation. Pour une condensation binaire, la concentration de la vapeur en écoulement libre est importante. Des concentrations plus élevées du composant le plus volatil tend à inhiber la condensation.

MEHRKOMPONENTEN-GRENZFLÄCHENKONDENSATION

Zusammenfassung—In dieser Arbeit wird ein einfaches laminares achsensymmetrisches Modell zur Untersuchung der Mehrkomponenten-Kondensation verwendet. Zusätzlich zu dem mit der Kondensation von Mehrkomponenten-Gemischen verbundenen komplizierten Phasengleichgewicht werden die Schubspannung an der Phasengrenze sowie der Stoff- und Energietransport betrachtet. Es wird gezeigt, daß ein nichtkondensierbares Gas den Kondensationsstrom an der Phasengrenze deutlich vermindert. Im Falle der Kondensation binärer Gemische ist die Konzentration der ungestörten Strömung sehr wichtig. Höhere Anteile der leichter flüchtigen Komponente führen zu einer Behinderung der Kondensation.

МНОГОКОМПОНЕНТНАЯ КОНДЕНСАЦИЯ НА МЕЖФАЗНОЙ ГРАНИЦЕ

Аннотация—Для исследования многокомпонентой конденсации применяется простая осесимметричная модель. Наряду со сложными состояниями фазового равновесия, характерными для многокомпонентной конденсации, учитываются также касательное напряжение и перенос массы и энергии на межфазной границе. Показано, что неконденсирующийся газ вызывает существенное уменьшение скорости конденсации на межфазной границе. Важным фактором конденсации бинарой смеси является концентрация пара в свободном потоке. При высоких концентрациях более летучего компонента наблюдается тенденция к подавлению конденсации.